Title: Electrodeposition of Epitaxial Co on $Ru(0001)/Al_2O_3(0001)$

Ryan Gusley[1], Kadir Sentosun[2], Sameer Ezzat[3], Kevin. R. Coffey[4], Alan C. West[1], Katayun Barmak[2]

Abstract

The 60 nm-thick Ru(0001) layer was deposited epitaxially onto $Al_2O_3(0001)$ by ultrahigh vacuum (UHV) sputter deposition at 500°C followed by a step anneal (ex situ) to 950°C. The Co layer was electrodeposited at room temperature from an acidic electrolyte (pH = 3.8) containing dilute Co metal ions. Previously unreported, evidence for the underpotential deposition (UPD) of Co on Ru(0001) is presented and was shown to affect the nucleation of Co during constant potential electrodeposition. This result demonstrates a strong interaction between Co and the Ru substrate necessary for epitaxial growth. Cross-sectional transmission electron imaging and diffraction confirmed the formation of an epitaxial layer of Co(0001) on Ru(0001) to practical thicknesses for interconnect gap-fill. This finding suggests the plausibility of electrodeposited, single crystal interconnects in future integrated circuit chips.

[1] Department of Chemical Engineering, Columbia University, New York, NY 10027

[2] Department of Applied Physics and Applied Mathematics, Columbia University, New York, NY 10027

[3] Department of Chemistry, College of Science, University of Mosul, Mosul, Iraq 41002

[4] Department of Materials Science and Engineering, University of Central Florida, Orlando, FL 32816

Background

Interconnect power consumption and RC delay are dominant issues for CMOS technology on integrated circuit (IC) chips. With the arrival of each new technology node, the dimensions of interconnects are scaled to accommodate an increase in device density. This scaling results in an increase of interconnect resistance measured as:

$$R = \rho \frac{L}{A} \quad [1]$$

where ρ is metal resistivity, L is interconnect length, and A is interconnect cross-sectional area. The power consumption resulting from polycrystalline copper (Cu) interconnects on an IC dominates the majority of power consumption in a semiconductor device.[1] As the line-width of Cu interconnects shrinks closer to the electron mean free path of the Cu, the resistivity ρ increases rapidly due to increased electron scattering at surfaces[2–6] and grain boundaries[2,5–8] in a phenomenon known as resistivity-size effect. It is approximated that the resistivity of a 10 nm-wide Cu interconnect line will be an order of magnitude larger than that of bulk Cu.[9] Cu remains the current choice of metal in interconnect technology due to its low bulk resistivity,[10] however, the metal possesses a large mean free path of 39 nm at room temperature.[11] This causes the metal to experience size effects at larger dimensions than a metal with a lower mean free path would. While research is being performed to improve the conductivity of Cu,[3,12,13] several alternative metals are being investigated.

Cobalt (Co) is one metal currently being investigated to replace Cu in interconnect technology.[4,14–16] While hexagonal close-packed (hcp) Co has higher intrinsic resistivity value at room-temperature ($\rho_{0,rt}$ = 6.2 μΩ-cm) than Cu ($\rho_{0,rt}$ = 1.7 μΩ-cm), the computed values of the mean free path of Co are lower (λ_{rt} = 11.8/7.7 nm, perpendicular/parallel to the hexagonal axis) making it a prime candidate to replace Cu in more narrow interconnect lines.[4] In interconnects

with an aspect ratio of 2:1, it has been calculated that Co will have a resistivity comparable to Cu at the 10 nm line-width despite having a bulk resistivity value more than 3 times larger.[12,17,18] Additionally, Co has a greater melting point of 1495 °C compared with Cu which has a melting point of 1085 °C. A correlation between higher melting points and greater resistance to electromigration has been established,[19] further justifying Co as a potential replacement for Cu.

While switching from Cu to Co interconnects at nano-scale interconnects may lead to improvements in conductivity, a polycrystalline Co interconnect will eventually encounter increased scattering at grain boundaries as well. This motivates an investigation of the fabrication of single crystal Co interconnects which has potential to be achieved through epitaxial deposition of Co onto a single crystal seed layer. Ruthenium (Ru) is currently being investigated to replace Ta/TaN as a barrier layer in future interconnects.[20] As a result, an investigation of the epitaxial deposition of single crystal Co from Ru(0001) is provided.

Epitaxial deposition of metals has been achieved with physical vapor deposition (PVD) processes that occur at ultra-high vacuum (UHV) and at elevated temperatures.[21,22] These conditions are not suitable for back-end-of-line (BEOL) processing which has a thermal budget of 400°C.[23] Alternatively, electrochemical methods are performed near room-temperature and are already practicable methods for IC fabrication. Co has been shown to demonstrate 3-D island nucleation and growth on Ru substrates through traditional constant potential electrodeposition which results in polycrystalline films.[24] Several electrochemical techniques, however, do exist for the epitaxial deposition of metallic thin films.

Surfactant-Mediated Growth (SMG), defect-mediated growth (DMG), and growth via surface-limited redox replacement (SLRR) have all demonstrated 2-D growth of epitaxial metal films to appreciable thicknesses.[25–28] These techniques involve the inclusion of a surfactant in the

deposition solution, most commonly toxic lead (Pb), complicating the solution chemistry and increasing the likelihood of incorporating the sacrificial metal into the desired metal film. Additionally, DMG and SLRR require a manipulation of applied potential throughout the course of the deposition process. Finally, of these three methods only growth via SLRR has been shown to deposit Co. These drawbacks make the aforementioned techniques challenging to implement for the deposition of single crystal interconnects, especially when minimal defects/contamination are desired.

In this paper we demonstrate the deposition of epitaxial Co onto a Ru(0001) seed layer. This was performed without the use of deposition techniques involving surfactants. Previously unreported, Co was shown to exhibit underpotential deposition (UPD) on Ru(0001). The strong interactions between Ru and Co that allow for UPD (i.e., involving work function, surface energy) influence the growth mode of Co resulting in the epitaxial deposition of Co as a single crystal to practical thicknesses for interconnect gap-fill. This is achieved despite a 6% lattice mismatch between the deposited hcp Co(0001) and the Ru(0001) substrate for the hexagon-on-hexagon orientation.

Methodology

Deposition and Surface Treatment of Ru(0001) Substrates.-Ru(0001) substrates were deposited epitaxially onto Al_2O_3(0001) by UHV sputter deposition at 500°C to a thickness of 60 nm followed by a step anneal to 950°C performed *ex situ*.[29] The coupons used for experimentation were laser cut and the surface area of the Ru substrate exposed to electrolyte was 0.5 cm^2. To pretreat the Ru prior to experimentation, the substrate was rinsed with acetone, ethanol and 18.2 MΩ-cm de-ionized (DI) water. Then, surface oxides from the Ru were reduced using a potentiostatic hold at -0.8 V vs. Ag/AgCl in 50 mM sulfuric acid (H_2SO_4, Sigma-Aldrich) for 120

s.[30]

Electrolyte.-The Co electrodeposition solution consisted of 1 mM cobalt sulfate heptahydrate ($CoSO_4.7H_2O$, Alfa Aesar, 99.999%), 0.125 mM sulfuric acid (H_2SO_4, Sigma-Aldrich), 10 mM potassium sulfate (K_2SO_4, Sigma-Aldrich), and 0.1 mM potassium chloride (KCl, Sigma-Aldrich). The solution pH was 3.8. The choice of electrolyte chemistry was influenced by Allongue, et al.[31] because of the authors' demonstration of depositing ultrathin layers of Co epitaxially in a layer-by-layer fashion on a gold (Au) substrate. Solution pH is a particularly important parameter as the pH can affect film morphology due to the parasitic hydrogen evolution reaction (HER) that happens on the substrate simultaneous to metal ion reduction.[32] The pH of the Co deposition electrolyte is also known to affect the crystal structure of Co.[33–36] In order to ensure the electrodeposition of hexagonal close packed (hcp) Co, which is desired for epitaxial growth on hcp Ru(0001), the pH was kept above 2.5.

A baseline solution was also used and consisted of the previously described electrolyte without Co metal ions present in any quantity (pH=3.8). Prior to electrochemical experiments, electrolytes were purged with argon (Ar) for one hour to remove oxygen from the solution. Solutions were made with 18.2 MΩ-cm deionized (DI) water (Direct-Q 3 UV-R, Millipore). All the chemicals used were reagent grade.

Deposition of Epitaxial Co Films.-An applied current was utilized in the electrodeposition of conformal, epitaxial Co films. During Co depositions, the electrolyte described previously was adjusted to include 10 mM Boric Acid (H_3BO_3, Sigma-Aldrich) as a buffer to avoid a local rise in pH near the electrode.[37] During the deposition process, solution agitation was provided through stir bar rotation at 150 RPM. A three-electrode set-up was used for all electrochemical experiments consisting of Ru(0001) as the working electrode, a platinum (Pt) wire counter electrode and a

saturated Ag/AgCl (Hach) reference electrode (E = +0.199 V vs. NHE). A Metrohm μAutolab Type III potentiostat was used for all electroanalytical measurements. All potentials are cited against saturated Ag/AgCl reference electrode unless otherwise stated.

Characterization of Electrodeposited Films.-The electrodeposited metal thin films were examined using electron microscopy. A FEI Talos F200X Transmission/Scanning Transmission Electron Microscope (S/TEM) was used for cross-sectional transmission electron imaging and diffraction in order to confirm the epitaxial deposition of the Co layer. Energy-dispersive X-ray spectroscopy (EDX) was used to determine the elemental composition of the films. Sample cross-sections were prepared using a focused ion beam (FIB). A Zeiss Sigma VP Scanning Electron Microscope (SEM) was used to examine the surface of the Ru substrates prior to electrodeposition.

X-ray diffraction (XRD) was performed on a Panalytical X'pert3 Powder XRD with a Cu x-ray source (λ = 1.54 Å) using a flat stage attachment and was used to quickly extract information about the crystal structure and orientation of the electrodeposited films. The XRD was operated at 45 kV and 40 mA. The diffraction pattern was collected between 2θ values of 30° to 100° with a $^{1}/_{16}$" divergence slit (FDS), $^{1}/_{32}$" anti-scattering slit (IASS), and a 10 mm mask. In order to avoid damaging the detector due to intense scattering from the single crystal substrate, the sample was orientated slightly off from the exact Bragg angle of Ru and sapphire reflections.

Results and Discussion

Fig. 1 shows cyclic voltammograms (CVs) of Ru(0001) in solutions with and without 1 mM $CoSO_4$ present. In both voltammograms, two reduction peaks are observed at -0.02 V and -0.21 V. The integration of charge under these two peaks was calculated as 260 $\mu C/cm^2$. While this value is in close agreement with the charge density associated with a one electron surface oxidation of the Ru(0001),[38] Ru surface oxides were reduced prior to performing the CV and the

solution has been purged with Ar. These peaks, therefore, are believed to be related to the adsorption (reduction) of underpotentially deposited hydrogen which is also a one electron reaction and is known to occur on Ru.[39] In the reverse scan, a large oxidation peak followed by a small, broad peak are present at -0.16 V and 0.15 V, respectively, and appear to be correlated to the H adsorption peaks. The oxidation of the Ru surface to RuOH is known to begin around 0.05 V vs. Ag/AgCl.[40] The first peak at -0.16 V is entirely negative of this potential while the peak at 0.15 V starts negative of the potential but extends positive of it. Considering both of these peaks begin at potentials negative of this value, the reaction is attributed to H desorption. Further negative of the H UPD reduction peaks, a third reduction peak is observed in both scans and corresponds to the diffusion limited reduction of protons in the hydrogen evolution reaction (HER), $H^+ + e^- \rightarrow \frac{1}{2} H_2$.[31,41] In the CV performed with 1 mM Co^{2+} included in the electrolyte, an additional reduction peak is observed at -0.96 V and two additional oxidation peaks are present at -0.43 V and -0.36 V. The reduction peak corresponds to the reduction of Co^{2+} to Co while the two oxidation peaks are related to the stripping of the electrodeposited Co. The small shoulder on the largest oxidation peak is claimed to be related to the oxidation of a hydrogen rich cobalt phase.[42] We propose that the Co oxidation peak at the more positive potential is the stripping of underpotentially deposited Co and present evidence supporting this claim later on. The HER occurs simultaneous to the reduction of Co making the onset of Co overpotential deposition (OPD) difficult to distinguish. The reversible potential of Co reduction was determined experimentally by measuring the open circuit potential (OCP) of Co electrodeposited to a thickness of 10 nm. The measurement was performed directly after electrodeposition and the OCP was determined as -0.58 V vs. Ag/AgCl.The Nernst potential of Co deposition from a Co^{2+} concentration of 1 mM is calculated as -0.57 V vs. Ag/AgCl. Good agreement is observed between the calculated Nernst potential of

Co and the value observed from the OCP measurement. Moving forward, the experimentally determined reversible potential of $E^{0}_{Co^{2+}/Co}$= -0.58 V vs. Ag/AgCl will be referenced.

Co UPD has been observed on platinum (Pt),[43] Au,[44] and glassy carbon electrodes (GCE)[45] but has not been reported on Ru. UPD is a self-limiting process that results in the deposition of a monolayer or (sub)monolayer of the depositing metal at potentials positive of bulk deposition, or OPD. In UPD metal-substrate pairs, the work function of the substrate is greater than that of the depositing metal.[46] The work function of Ru(0001) is reported between Φ = 4.71-5.84 eV[47,48] while the work function of Co(0001) between Φ = 5.26-5.81eV.[47–49] With such large variability of the two work functions reported in literature, experimental methods were used to determine if Co underpotentially deposits on Ru(0001).

The feasibility of Co UPD on Ru(0001) was investigated through the use of a potentiostatic hold followed by linear sweep voltammetry (LSV) performed in the anodic direction and is presented in Fig. 2. In this experiment, a potential of -0.56 V was held for 60 seconds. This potential, $E_{Co\text{-}UPD}$, is 20 mV positive (η = +20 mV) of the experimentally determined Nernst reduction potential of Co. Following this potential hold, an LSV was performed from -0.56 V to 0.3 V at a scan rate of 20 mV/s to oxidize any adsorbed species resulting from the potential hold from the surface of the Ru electrode. The LSV experiments were performed from solutions with and without 1 mM Co^{2+} present. H UPD oxidation peaks are present in the LSVs from both solutions centered at -0.16 V and 0.15 V. The LSV with Co^{2+} has two distinct oxidation peaks at -0.44 V and -0.40 V. Considering the potential hold takes place positive of the Nernst potential of Co deposition, the two oxidation peaks correspond to the stripping of underpotentially deposited Co. Additionally, a large disparity in current density is seen at the beginning of the LSV. This current is predominantly associated with hydrogen evolution. Ru is a superior catalyst to Co for

HER as Ru is a Pt-group metal. This suppression of HER current, can be explained by the presence of UPD Co on the Ru substrate.[50] Ru, therefore, shows a co-adsorption of underpotentially deposited Co and H atoms when the potential is held at $E_{Co\text{-}UPD}$.

A quantitative value of Co UPD surface coverage is difficult to obtain without adjusting the pH due to HER and H UPD occurring in the same potential range.[51] The theoretical charge density associated with the stripping of a Co monolayer is 590 μC/cm^2.[31] From Fig. 2, the resulting charge density from stripping associated with Co UPD was calculated to be less than a full Co monolayer. As the Co oxidizes, Ru becomes accessible for HER and H adsorption, contributing a negative current density. Thus, the charge measured through this technique is likely an underestimate.

The potentials of the Co UPD oxidation peaks displayed in Fig. 2 are offset from the second Co oxidation peak from the CV in Fig. 1. An additional LSV at a slower rate, presented in Fig. 3, was performed to show how the Co oxidation peaks change after varying polarization times at -0.75 V (η = -70 mV). The asymmetric peak at more negative potentials increases in size with longer potential holds. This peak is associated with the oxidation of overpotentially deposited or bulk Co. A smaller and sharper peak is present at -0.41 V that does not change size or change peak potentials with longer polarizations. This peak is related to the oxidation of UPD Co. Additionally, at this slower scan rate the Co UPD stripping peak potential shows better agreement with the Co UPD peaks found in Fig. 2. The difference observed in the CV is likely because at the faster scan rate the OPD Co was not fully stripped before the UPD stripping potential was reached which caused the Co UPD to strip at more positive potentials.

The kinetics of the Co underpotential deposition reaction were studied by determining the time it takes for underpotentially deposited Co to reach its maximum surface coverage θ_{max}. The

stripping current profile shown in Fig. 2 after a 60 second long hold at $E_{Co\text{-}UPD}$ is fully established and the calculated charge density of stripping does not increase with increasingly long polarization times. At this point of maximum charge density, it is assumed that the surface coverage of UPD Co is at θ_{max}. Additionally, in the baseline solution, the stripping current profile due to H UPD after a potential hold at $E_{Co\text{-}UPD}$ is completed at t ~5 seconds. Therefore, after 5 seconds any change in charge density measured during the LSV should be attributed to a change in Co surface coverage. Based on these assumptions, the following relationship is established:

$$\frac{\theta}{\theta_{max}} = \frac{q}{q_{max}} \quad [2]$$

Where q is the measured charge density from the LSV performed after potentiostatic holds of less than 60 seconds and q_{max} is the maximum charge density calculated from the LSV when the hold at $E_{Co\text{-}UPD}$ is 60 seconds. The Co UPD surface coverage relative to the maximum surface coverage as a function of time is shown in Fig. 4. The stripping charge density, and therefore Co UPD surface coverage, begins to saturate at $t > 20$ seconds.

A potential step was used to show the effect of Co UPD on the nucleation and growth of Co films in Fig. 5.[52] Results are plotted as $-i$ [mA/cm^2] versus t [seconds] to clearly see the current time transient resulting from the potential step. The Ru(0001) electrode was stepped to -0.8 V, an overpotential of -220 mV for Co OPD, from three different initial potential holds for 20 seconds. The first initial potential was chosen and -0.4 V (η = +180 mV) where H is fully adsorbed onto Ru(0001). At this potential, Co is not present on the Ru surface due to OPD or UPD. The second initial potential was chosen as -0.56 V or $E_{Co\text{-}UPD}$ (η = +20 mV), a potential suitable for Co UPD. The current transient after the step to η = -220 mV from η = +180 mV resulted in a clear peak followed by an eventual decay of current density to a steady-state value corresponding to the nucleation and growth process of Co. When stepped from $E_{Co\text{-}UPD}$, the current directly decays to a

steady-state value and no such peak is observed. A final initial potential hold was chosen as -0.6 V (η = -20 mV), negative of the Nernst potential of Co. When stepped to η = -220 mV, the current density again decayed directly to a steady value. It appears the presence of Co UPD prior to the application of an overpotential to Co reduction possibly obviates the nucleation step for Co deposition.

A second potential step experiment was performed to establish the kinetics of the Co UPD reaction. Fig. 6 shows the current transients resulting from a potential step to η = -230 mV after a potentiostatic hold at $E_{Co\text{-}UPD}$ for varying times. For holds at $E_{Co\text{-}UPD}$ of 10 seconds or less, the current transient resembles that observed during Co nucleation and growth. As the time of hold increases to 20 seconds and longer, a peak is no longer observed. The difference in current transient for times longer than 20 seconds is negligible, signifying that a maximum coverage of underpotentially deposited Co is reached after about 20 seconds. This supports the results shown in Fig. 4.

A Co film was electrodeposited on 60 nm thick Ru(0001) / Al_2O_3(0001) substrates at -100 $\mu A/cm^2$ for 2700s which resulted in an average potential of -0.80 V vs. Ag/AgCl. A constant current was applied during the deposition for a precise control of deposition rate and thickness. During the galvanostatic deposition, the potential quickly reached values between 10-40 mV positive of the Nernst potential of Co^{2+} reduction and remained there for several seconds before shifting to more negative values. This suggests that the Co UPD monolayer was deposited before subsequent layers. The current efficiency was calculated as 27% with a majority of current going toward HER even though no hydrogen bubbles were observed visually during electrodeposition. The applied current density was selected as it ensured that the current density attributed to Co OPD was less than the limiting current density of the reaction with 1 mM $CoSO_4$ ($i_L \sim 100\ \mu A/cm^2$).

The film structure and morphology were studied using transmission electron microscopy (TEM) after cross-section sample preparation using FIB. A bright field TEM image of the Co film deposited for 2700 s and electron diffraction pattern of the Co and Ru layers are shown in Fig. 7. The Co film thickness is measured to be 25 nm. By analyzing different regions, it is observed that the Co film is continuous on the surface of the Ru. The film roughness does not exceed the roughness of the Ru film with exclusion of two locations where Co deposition appears to have been inhibited. This may be due to the presence of hydrogen bubbles blocking Co growth during electrodeposition. Selected area electron diffraction (SAED) patterns acquired from the film is displayed as an inset in Fig.7 a). The analysis of SAED patterns revealed that the Ru is in $[10\bar{1}0]$ zone axis. In the diffraction pattern (DP), a second reflection is present next to each reflection from Ru (highlighted in figure inset). This reflection is from the Co layer and the d-spacing measured from the additional reflections are in good agreement with the reflections in XRD pattern displayed in Fig. 8 where both results indicate that the Co layer is in hcp phase. Moreover, these reflections suggest that Co is also in same zone axis as Ru. This analysis clearly show that an epitaxial relation is present between the Co and Ru layers where Co[0001] || Ru[0001] and Co$[1\bar{2}10]$ || Ru$[1\bar{2}10]$, i.e. the orientation relationship is of hexagon-on-hexagon or unrotated honeycomb. This should be contrasted with the 30° rotated honeycomb of Ru on sapphire where Ru$[11\bar{2}0]$ || $Al_2O_3[10\bar{1}0]$.[53]

A second sample was deposited to the same thickness at a lower current density of -80 $\mu A/cm^2$ and the film quality was observed. At this current density, the current efficiency dropped to 14% and the average potential throughout the galvanostatic deposition decreased to -0.78 V vs. Ag/AgCl. Electron diffraction and TEM cross-section are present in Fig. 7 b) and d). The variation in contrast between the two films is due to a difference in the thickness of the electron transparent sections. This sample shows no large voids in the Co layer such as those shown previously,

however, there are smaller regions where Co deposited to a slightly lesser thickness. This is likely an effect of the ruthenium surface quality. Using scanning electron microscopy (SEM), small scratches resulting from sample handling were found and may have inhibited Co growth. This issue is likely resolved with a more pristine Ru wafer. Overall, the Co layer showed minimal roughness and only slightly exceeded the roughness of the underlying Ru layer. From the cross-sectional TEM image, defects in the Ru film are found to propagate into the electrodeposited Co layer. If Co was electrodeposited from a thinner Ru film with no defects, the observed defects in the Co film should not be present. Further analysis by means of HRTEM imaging is also shown in Fig. 7 e) and f). The atomic planes displayed in the micrographs are the (0002) planes. HRTEM shows an epitaxial relation between the Co(0001) and Ru(0001) as well as between Ru(0001) and Al_2O_3(0001). At the interface between Co and Ru, the epitaxial relationship is remarkably clear and it is difficult to distinguish the two layers. EDS analysis shown in Fig. 9 confirms the presence of continuous Co layer on Ru. It is observed that no alloy formation or intermixing between the layers is present. The spectrum appears as expected with no unexpected elemental signals. Cu is present in the spectrum because the sample was mounted on a Cu TEM grid.

Adhesion of the Co thin film was tested by sticking tape to the sample and peeling the tape. Adhesion only failed at the interface of Ru(0001)/Al_2O_3(0001) and never at the interface of Co(0001)/Ru(0001), suggesting good adhesion between the two metal films.

The presented work showcases the ability to use electrodeposition to deposit an epitaxial, single crystal metallic layer provided there is a conductive, single crystal seed layer. To implement this technique into the interconnect fabrication process, it is therefore necessary to have access to a single crystal, conductive seed layer. An example of such a layer is a silicide contact metallization formed epitaxially on the single crystal base semiconductor wafer.[54] Intermediate

epitaxial layers may be grown atop the silicide to improve the lattice matching to the interconnect metal of interest. In a Damascene-like process, the electrodeposited epitaxial interconnect metal will then be grown from the bottom of the vias upwards to the next metallization layer. Continued lateral growth from these vias until impingement of growth from adjacent vias will allow trenches to be filled with the single crystal interconnect metal connecting devices. Subsequent planarization will then define each layer of the interconnect metallization. The lateral growths from multiple vias will have a common crystallographic orientation derived from the single crystal substrate below, and this is expected to result in an absence of grain boundaries where these growths impinge, although other planar defects (e.g., anti-phase boundaries) may be present.

Conclusions

Two-dimensional growth of epitaxial Co was performed onto Ru(0001) without the use of surfactants. This was achieved through constant current deposition at low current density from a solution of dilute metal ions. The epitaxial and single crystal nature of the electrodeposited Co was confirmed through HRTEM and electron DP. The two electrodeposited Co(0001) films are shown to be conformal and continuous on the Ru substrate. Evidence of Co UPD is provided as well, which demonstrates strong interaction between Ru and the electrodepositing Co necessary for epitaxial deposition. These findings suggest the plausibility of single crystal interconnect fabrication by electrochemical methods in future IC chips.

Acknowledgments

This material is based on work supported by the National Science Foundation (ECCS-1740270 and 1740228) and the Semiconductor Research Corporation (task 2764.001 and 2764.003). This work was carried out in part in the Electron Microscopy and Shared Materials

Characterization Laboratories of Columbia Nano Initiative (CNI) Facilities at Columbia University.

References

1. D. H. Albonesi, A. Kodi, and V. Stojanovic, *Final Report of the NSF Sponsored Workshop on Emerging Technologies for Interconnects*, (2013).

2. K. Barmak, X. Liu, A. Darbal, N. T. Nuhfer, D. Choi, T. Sun, A. P. Warren, K. R. Coffey, and M. F. Toney, *J. Appl. Phys.*, **120**, 065106 (2016).

3. P. Zheng, T. Zhou, and D. Gall, *Semicond. Sci. Technol.*, **31**, 055005 (2016).

4. D. Gall, *J. Appl. Phys.*, **119**, 085101 (2016).

5. T. Sun, B. Yao, A. P. Warren, K. Barmak, M. F. Toney, R. E. Peale, and K. R. Coffey, *Phys. Rev. B*, **79**, 41402 (2009).

6. K. Barmak, T. Sun, and R. Coffey, in *AIP Conference Proceedings*, **1300**, 12 (2010).

7. T. Zhou and D. Gall, *Phys. Rev. B*, **97**, 165406 (2018).

8. A. F. Mayadas and M. Shatzkes, *Phys. Rev. B*, **1**, 1382 (1970).

9. C. Pan and A. Naeemi, *IEEE Electron Device Lett.*, **35**, 250 (2014).

10. S. P. Murarka, R. J. Gutmann, A. E. Kaloyeros, and W. A. Lanford, *Thin Solid Films*, **236**, 257 (1993).

11. F. Chen and D. Gardner, *IEEE Electron Device Lett.*, **19**, 508 (1998).

12. P. Y. Zheng, R. P. Deng, and D. Gall, *Appl. Phys. Lett.*, **105**, 131603 (2014).

13. M. César, D. Gall, and H. Guo, *Phys. Rev. Appl.*, **5**, 54018 (2016).

14. E. Milosevic, S. Kerdsongpanya, and D. Gall, in *IEEE Nanotechnology Symposium (ANTS)*, IEEE (2018).

15. N. Bekiaris, Z. Wu, H. Ren, M. Naik, J. H. Park, M. Lee, T. H. Ha, W. Hou, J. R. Bakke, M. Gage, Y. Wang, and J. Tang, in *IEEE International Interconnect Technology Conference (IITC)*, IEEE (2017).

16. E. Milosevic, S. Kerdsongpanya, M. E. Mcgahay, A. Zangiabadi, K. Barmak, and D. Gall, *J. Appl. Phys.*, **125**, 245105 (2019).

17. R. W. Powell, R. P. Tye, and M. J. Woodman, *J. Less-Common Met.*, **12**, 1 (1967).

18. E. Milosevic, S. Kerdsongpanya, A. Zangiabadi, K. Barmak, K. R. Coffey, and D. Gall, *J. Appl. Phys.*, **124**, 165105 (2018).

19. C. Adelmann, L. G. Wen, A. P. Peter, Y. K. Siew, K. Croes, J. Swerts, M. Popovici, K. Sankaran, G. Pourtois, S. Van Elshocht, J. Bommels, and Z. Tokei, in *International Interconnect Technology Conference (IITC)*, IEEE (2014).

20. R. Bernasconi and L. Magagnin, *J. Electrochem. Soc.*, **166**, D3219 (2019).

21. A. Y. Cho and J. R. Arthur, *Prog. Solid State Chem.*, **10**, 157 (1975).

22. S. I. Stenin and A. I. Toropov, in *Growth of Crystals*, Springer US (1991).

23. J. Schmitz, *Surf. Coatings Technol.*, **343**, 83 (2018).

24. A. Sahari, A. Azizi, N. Fenineche, G. Schmerber, and A. Dinia, *Mater. Chem. Phys.*, **108**, 345 (2008).

25. Seongpil Hwang, A. Ilwhan Oh, and J. Kwak, **123**, 7176 (2001).

26. K. Venkatraman, Y. Dordi, and R. Akolkar, *J. Electrochem. Soc.*, **164**, D104 (2017).

27. K. Sieradzki, S. Brankovic, Dimitrov, and N. Dimitrov, *Science*, **284**, 138 (1999).

28. D. Wu, D. J. Solanki, A. Joi, Y. Dordi, N. Dole, D. Litvnov, and S. R. Brankovic, *J. Electrochem. Soc.*, **166**, D3013 (2019).

29. E. Milosevic, S. Kerdsongpanya, A. Zangiabadi, K. Barmak, K. R. Coffey, and D. Gall, *J. Appl. Phys.*, **124**, 165105 (2018).

30. U. Emekli and A. C. West, *Electrochim. Acta*, **54**, 1177 (2009).

31. P. Allongue, L. Cagnon, C. Gomes, A. Gündel, and V. Costa, *Surf. Sci.*, **557**, 41 (2004).

32. D. R. Gabe, *J. Appl. Electrochem.*, **27**, 908 (1997).

33. O. E. Kongstein, G. M. Haarberg, and J. Thonstad, *J. Appl. Electrochem.*, **37**, 675 (2007).

34. S. Nakahara and S. Mahajan, *J. Electrochem. Soc.*, **127**, 283 (1980).

35. O. Karaagac, H. Kockar, and M. Alper, *J. Supercond. Nov. Magn.*, **24**, 801 (2011).

36. A. Vicenzo and P. L. Cavallotti, *Electrochim. Acta*, **49**, 4079 (2004).

37. L. B. Harris, *J. Electrochem. Soc.*, **120**, 1034 (1973).

38. J. X. Wang, N. S. Marinković, H. Zajonz, B. M. Ocko, and R. R. Adžić, *J. Phys. Chem. B*, **105**, 2809 (2001).

39. B. Łosiewicz, M. Martin, C. Lebouin, and A. Lasia, *J. Electroanal. Chem.*, **649**, 198 (2010).

40. C. L. Green and A. Kucernak, *J. Phys. Chem. B*, **106**, 1036 (2002).

41. E. Gómez, R. Pollina, and E. Vallés, *J. Electroanal. Chem.*, **386**, 45 (1995).

42. J. S. Santos, R. Matos, F. Trivinho-Strixino, and E. C. Pereira, *Electrochim. Acta*, **53**, 644 (2007).

43. L. H. Mendoza-Huizar and C. H. Rios-Reyes, *J. Solid State Electrochem.*, **15**, 737 (2011).

44. L. . Mendoza-Huizar, J. Robles, and M. Palomar-Pardavé, *J. Electroanal. Chem.*, **521**, 95 (2002).

45. L. H. Mendoza-Huizar, C. H. Rios-Reyes, M. Rivera, and C. A. Galan-Vidal, *Adv. Tech Mat. Mat. Proc. J.*, **8**, 152 (2006).

46. D. M. Kolb, M. Przasnyski, and H. Gerischer, *J. Electroanal. Chem. Interfacial Electrochem.*, **54**, 25 (1974).

47. H. L. Skriver and N. M. Rosengaard, *Phys. Rev. B*, **46**, 7157 (1992).

48. H. B. Michaelson, *J. Appl. Phys.*, **48**, 4729 (1977).

49. S. Saito, K. Takeda, T. Soumura, T. Tani, and T. Maeda, *Phys. Status Solidi*, **142**, K29 (1994).

50. X. Liu, K. Venkatraman, and R. Akolkar, *J. Electrochem. Soc.*, **165**, B9 (2018).

51. A. El-Shafei, *J. Electroanal. Chem.*, **447**, 81 (1998).

52. G. Gunawardena, G. Hills, I. Montenegro, and B. Scharifker, *J. Electroanal. Chem.*, **138**, 225 (1982).

53. S. Yamada, Y. Nishibe, M. Saizaki, H. Kitajima, S. Ohtsubo, A. Morimoto, T. Shimizu, K. Ishida, and Y. Masaki, *Jpn. J. Appl. Phys.*, **41**, L206 (2002).

54. X. Gao, J. Andersson, T. Kubart, T. Nyberg, U. Smith, J. Lu, L. Hultman, A. J. Kellock, Z. Zhang, C. Lavoie, and S.-L. Zhang, *Electrochem. Solid-State Lett.*, **14**, H268 (2011).

Figures

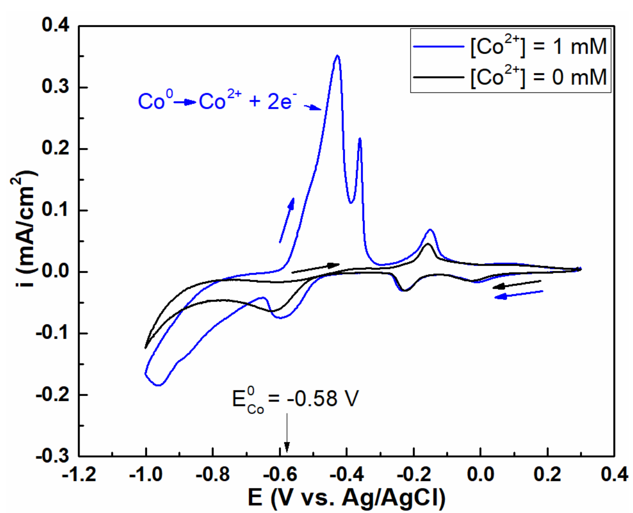

Figure 1. Cyclic voltammograms collected on a Ru(0001) substrate from solutions with (blue) and without (black) 1 mM $CoSO_4$, scan rate of 20 mV/s.

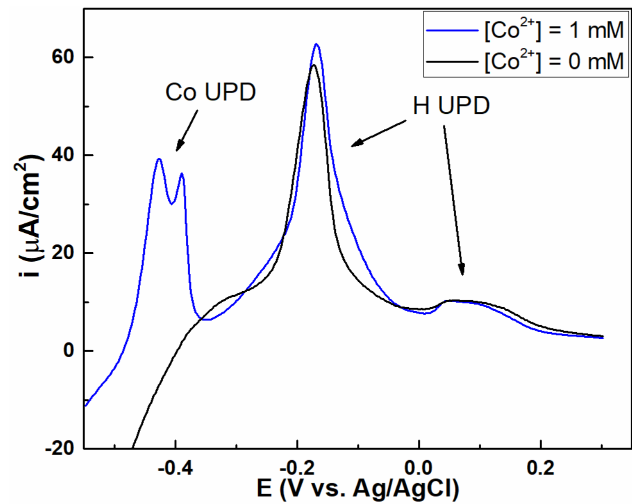

Figure 2. Linear sweep voltammograms on Ru(0001) substrate after hold at $E_{Co\text{-}UPD}$ (E = -0.56 V) for 60 seconds from solutions with (blue) and without (black) 1 mM $CoSO_4$, scan rate of 20 mV/s.

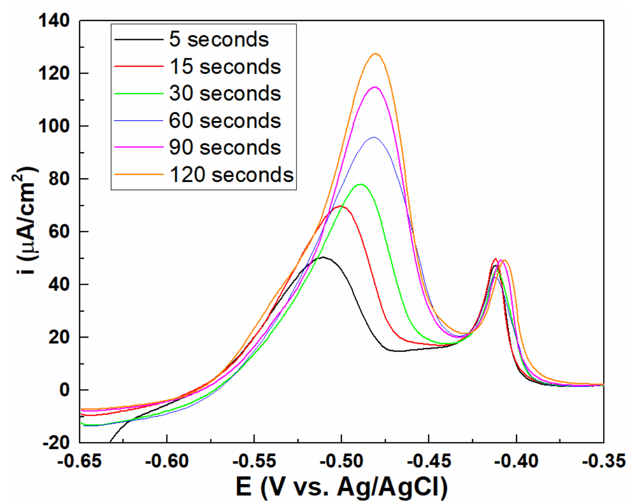

Figure 3. Linear sweep voltammograms on Ru(0001) substrate after increasing potentiostatic hold times at -0.75 V, scan rate of 5 mV/s.

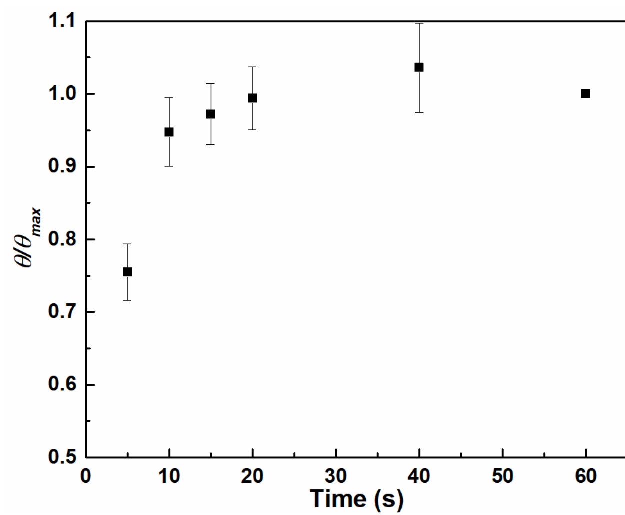

Figure 4. Co UPD surface coverage relative to maximum Co UPD surface coverage as a function of time. Underpotentially deposited Co reaches its maximum coverage after a 20 second hold at $E_{Co\text{-}UPD}$ (E = -0.56 V).

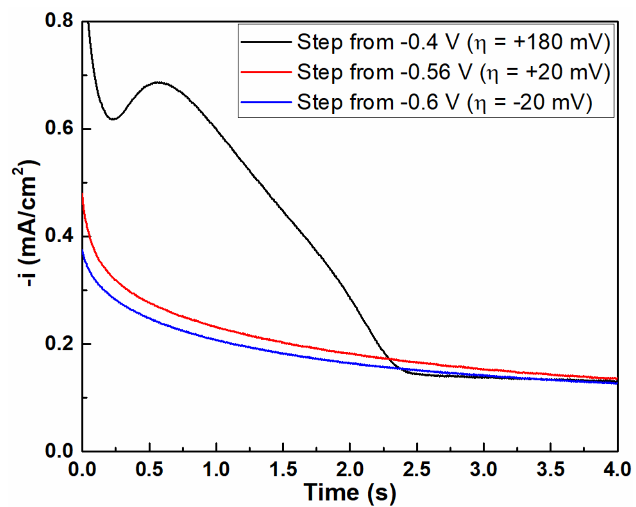

Figure 5. Current transients for Co electrodeposition on Ru(0001) substrate at -0.8 V after different initial holds. Initial holds of -0.4 V, -0.56 V and -0.6 V were performed for 20 seconds. Current transient from potential step on bare Ru substrate typical of nucleation and growth. Potential step after hold at $E_{Co\text{-}UPD}$ (E = -0.56 V) and -0.6 V results in a direct decay of current density signifying a deviation from nucleation.

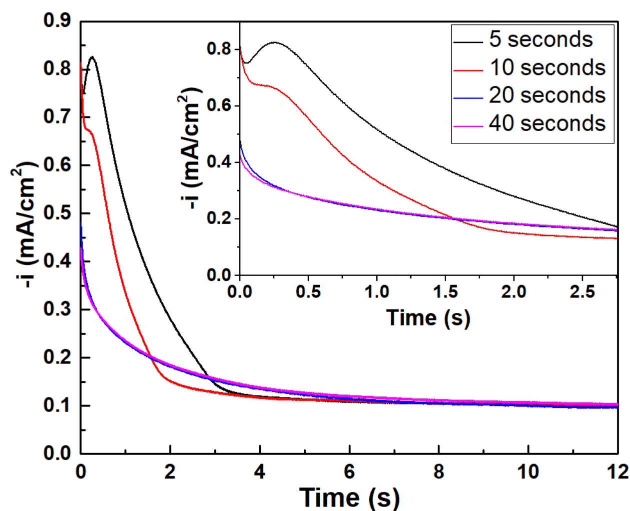

Figure 6. Current transients for Co electrodeposition on Ru(0001) substrate at -0.8 V after a potential hold at $E_{Co\text{-}UPD}$ (E = -0.56 V) for 5, 10, 20 and 40 seconds. Current transient deviates from nucleation and growth with longer holds at $E_{Co\text{-}UPD}$. Co UPD monolayer formed after about 20 seconds.

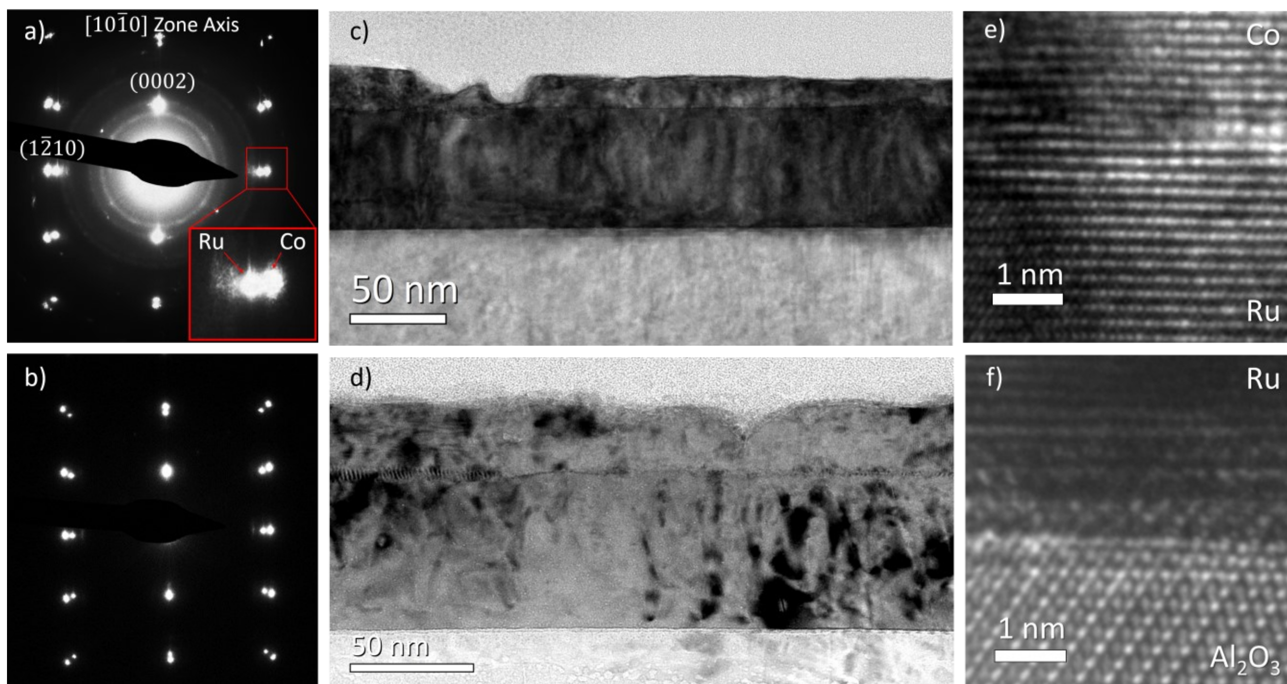

Figure 7. Electron diffraction patterns and cross-sectional TEM images are shown for Co electrodeposited at -100 μA/cm^2 (a & c) and at -80 μA/cm^2 (b & d) on Ru(0001). Diffraction patterns are in the [10$\bar{1}$0] zone axis. In both films, Co was deposited epitaxial to Ru(0001). HRTEM images are provided of the interface between Co and Ru(0001) (e) as well as Ru(0001) and Co(0001) (f).

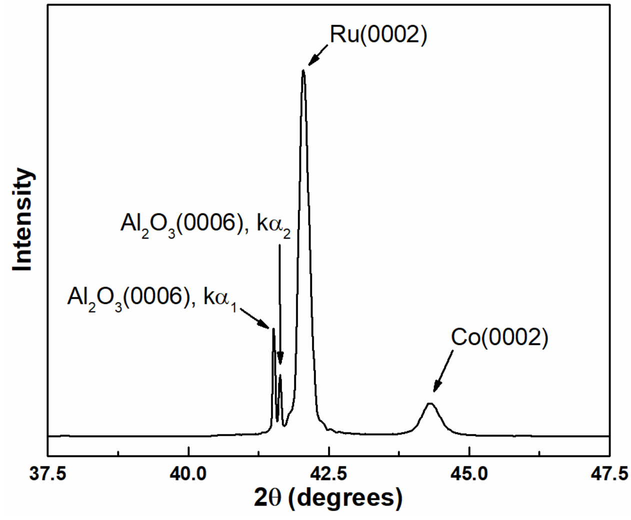

Figure 8. XRD of Co film electrodeposited onto Ru(0001)/Al_2O_3(0001) at -80 μA/cm^2. Reflection for Co(0002) present showing Co layer is hcp.

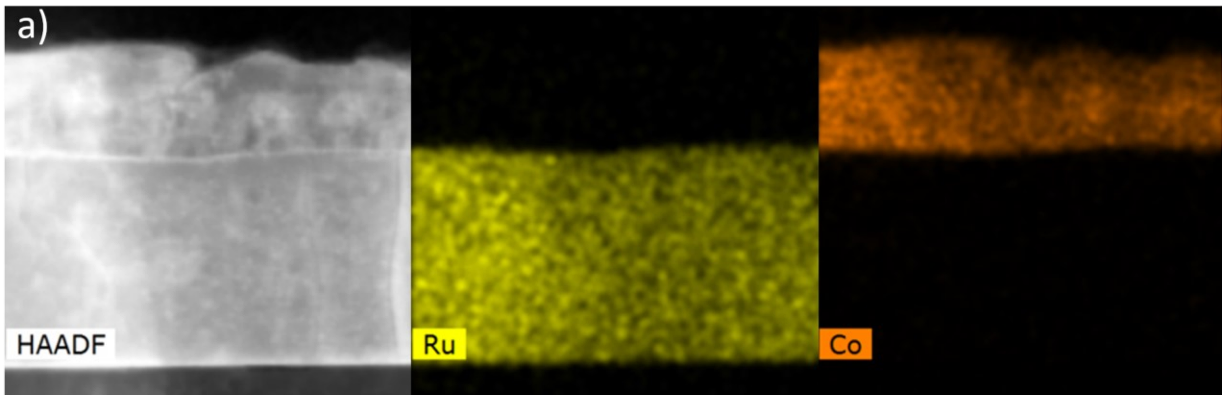

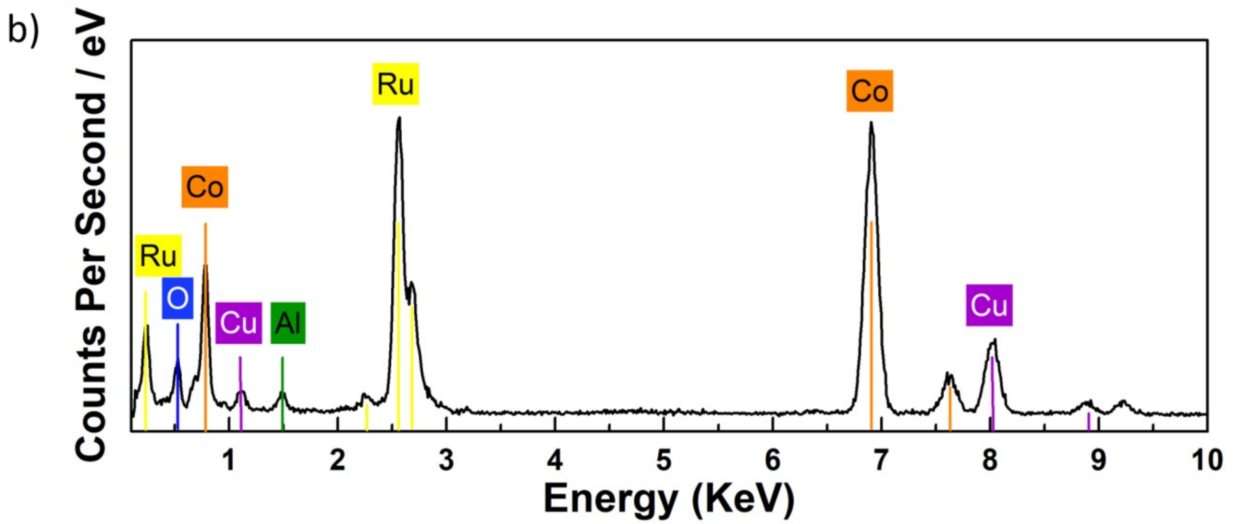

Figure 9. EDS was performed on Co electrodeposited at -80 μA/cm^2 on Ru(0001). EDS map (a) and the spectrum (b) is provided. EDS confirms presence of Co layer and shows no intermixing between the Co film and Ru(0001) substrate. EDS spectrum shows expected elemental signals.